Effect of Magnetic Field Ripple on ECCD in Heliotron J

K. Nagasaki 1), G. Motojima 2), S. Kobayashi 1), S. Yamamoto 1), T. Mizuuchi 1), H. Okada 1), K. Hanatani 1), S. Konoshima 1), K. Masuda 1), K. Kondo 3), Y. Nakamura 3), S. Watanabe 3), K. Mukai 3), K. Hosaka 3), K. Kowada 3), S. Mihara 3), Y. Yoshimura 2), Y. Suzuki 2), A. Fernández 4), A. Cappa 4), F. Sano 1)

1) Institute of Advanced Energy, Kyoto University, Gokasho, Uji, Kyoto, Japan
2) National Institute for Fusion Science, Toki, Gifu, Japan
3) Graduate School of Energy Science, Kyoto University, Kyoto, Japan
4) Laboratorio Nacional de Fusión, EURATOM-CIEMAT, Spain

e-mail address: nagasaki@iae.kyoto-u.ac.jp

Abstract. Electron cyclotron current drive (ECCD) experiment has been made in the helical-heliotron device, Heliotron J. A wide configuration scan shows that the EC driven current is strongly dependent on the magnetic ripple structure where the EC power is deposited. As the EC power is deposited on the deeper ripple bottom, the EC driven current flowing in the Fisch-Boozer direction decreases, and the reversal of directly measured EC driven current is observed. High energy electrons are suppressed for ripple bottom heating, indicating that generation and confinement of trapped electrons have an important role on ECCD. For ripple top heating, the typical ECCD efficiency is estimated $\gamma=n_e I_{EC} R/P_{EC} = 0.8\times10^{17}$ A/Wm^2 and $\zeta=e^3 n_e I_{EC} R/\varepsilon_0^2 P_{EC} T_e$, =0.05. The normalized ECCD efficiency is found to be independent on the absorbed EC power for both ripple top and bottom heating cases.

1. Introduction

Non-inductive current has an important role on realization of high performance plasmas and sustainment of steady state plasmas in toroidal fusion devices. In stellarator/heliotron (S/H) systems, no Ohmic current is required for equilibrium since the confinement magnetic field is generated by external coils. However, it is known that non-inductive current flows as well as in tokamaks. Finite plasma pressure drives bootstrap current, and tangential neutral beam injection (NBI) generates so called Ohkawa current, which modify rotational transform profile, resulting that the equilibrium and stability is affected [1]. The non-inductive current also modifies the edge field topology and divertor performance, which has been observed in Heliotron J [2]. Furthermore, transition onset to an improved confinement mode in NBI plasmas has been observed in relation to the non-inductive current in Heliotron J [3].

Electron cyclotron current drive (ECCD) is recognized as a useful scheme for stabilizing magnetohydrodynamic (MHD) instabilities and analyzing heat and particle transport. For example, in large tokamaks such as JT-60U, neoclassical tearing mode has been stabilized by localized ECCD, leading to the improvement of normalized beta [4]. In S/H systems, ECCD is expected as a useful scheme to avoid dangerous rational surface by cancelling the bootstrap current particularly in low shear devices. Recently research on ECCD has been active in S/H systems in order to understand the ECCD physics and to investigate the applicability of ECCD to the control of plasma equilibrium and stability. Experimental research on ECCD has been performed in Heliotron J [5], W7-AS [6], TJ-II [7], CHS [8] and LHD [9]. Comparative studies among some devices have also been performed under the framework of international collaboration, and common phenomena connected with injection angle dependence and ECCD efficiency has been observed [10].

From the viewpoint of diagnostics, the S/H systems have advantage of precise measurement of the EC driven current with the accuracy of the order of less than 1 kA by using

conventional Rogowski coils because of no Ohmic current. On the other hand, estimation of the EC current is not so simple in tokamaks since a large amount of Ohmic current flows, and the effects of toroidal electric field and plasma resistivity have to be taken into account. Comparison of the experimental results between tokamaks and helical systems gives us deeper understanding of ECCD physical mechanism in toroidal devices.

This paper presents recent experimental results on ECCD in Heliotron J. The role of high energy electrons on the ECCD related to the magnetic trapping is discussed. This paper is organized as follows. The experimental set up including the ECH/ECCD system is described in Sec. 2. The experimental results, especially the dependence on magnetic field structure are shown in Sec. 3. The ECCD efficiency is also discussed. Summary is given in Sec. 4.

2. Experimental Setup

Heliotron J is a medium-sized plasma experimental device, belonging to S/H systems [11][12]. The device parameters are the plasma major radius, R=1.2 m, the averaged minor radius a=0.1-0.2 m, the rotational transform $\iota/2\pi$=0.3-0.8, and the maximum magnetic field strength on the magnetic axis, B=1.5 T. The coil system is composed of an L = 1, M = 4 helical coil, two types of toroidal coils A and B, and three pairs of vertical coils. Here, L is the pole number of the helical coil and M is the pitch number of the field along the toroidal direction. A wide configuration scan can be produced on the Heliotron J by varying the current ratios in each coil, making it possible to investigate the properties of non-inductive current. As illustrated in Fig. 1, the magnetic field ripple defined by the ratio of the magnetic field at the straight section (ϕ=0 deg) to that at the corner section (ϕ=45 deg) , $h=B_{str}/B_{cor}$, ranges from 0.78 to 1.06 in the experiment reported here. The magnetic field has a structure from local maximum (ripple top heating) to local minimum (ripple bottom heating) at the EC power deposition position with keeping the plasma volume and rotational transform almost constant. The ratio ε_b is defined by B_{04}/B_{00}, where B_{04} and B_{00} is the bumpiness and uniform components of the magnetic field strength in Boozer coordinates, respectively. This bumpiness component ε_b, which is introduced as a third knob for controlling the neoclassical transport, is varied by controlling the currents in toroidal coils A and B.

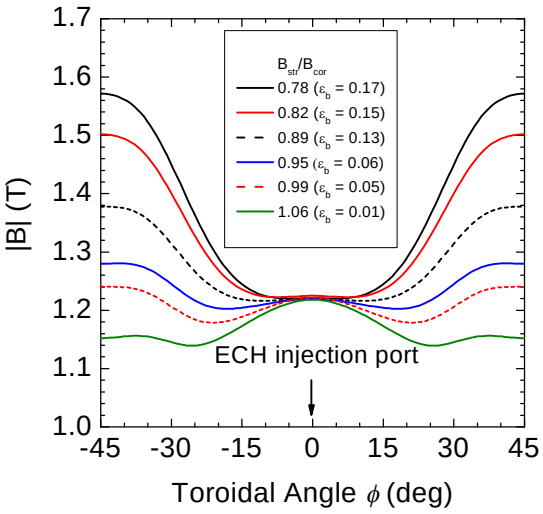

FIG. 1. Magnetic field profile along magnetic axis in Heliotron J. The bumpiness is scanned from ε_b=0.01 to 0.17, enabling ripple top and ripple bottom heatings.

A 70-GHz ECH system is used for studying non-inductive current in Heliotron J. Plasmas are produced and heated by the 70-GHz second harmonic X-mode ECH, which has a cut-off density of 3.0×10^{19} m^{-3}. In this study, injected powers of up to 440 kW are used and the maximum pulse length is 160 msec. An unfocused Gaussian beam is launched from the top of the torus in the “straight” section (ϕ=0 deg) where the flux surfaces are bean-shaped, and the B-contour forms a saddle-type structure. Although the wave beam is injected perpendicularly with respect to the equatorial plane, it crosses the resonance layer obliquely because of the

3-D magnetic field structure, resulting in a finite parallel refractive index $N_{\|}$ of 0.44 that drives the EC current. The polarization of injected waves is fixed with the X-mode. The central electron and ion temperatures are in the ranges 0.3-1.0 keV and 0.15-0.2 keV, respectively. The single pass absorption rate estimated from transmitted wave measurements [13] was found to be approximately 90 % at low density, 0.5×10^{19} m^{-3}, and it was consistent with that calculated by a ray tracing coed, TRECE [14], indicating that single pass absorption is the main contribution to plasma heating. [5][15].

The total toroidal current is measured by Rogowski coils wound on the inner wall of the poloidal cross-sections at two different toroidal angles, that is, the corner and the straight sections. We confirmed that the toroidal currents measured by two Rogowski coils were almost the same. An L_p/R_p time is about 100 - 200 msec for the Heliotron J plasma parameters, where L_p and R_p are the plasma inductance and resistance. In the experiment reported here, the measured toroidal current became saturated within the pulse length for $n_e > 0.5\times10^{19}$ m^{-3}, but it continued to increase during discharge at lower densities so that the current is underestimated in the low-density regime.

The magnetic field, B = 1.25 T, is located on the magnetic axis at $\omega_0/\omega = 0.50$, where ω_0 is the electron cyclotron frequency on the axis in the straight section and ω is the injected wave frequency. The ray tracing calculation shows that under this condition, the EC power is deposited off-axis for $\rho\sim0.3$ due to the Doppler shift resonance, $\omega - k_{\|}v_{\|} = 2\omega_{ce}$, where $k_{\|}$ is the parallel component of the wavenumber, $v_{\|}$ is the parallel velocity component and ω_{ce} is the electron cyclotron frequency. When the magnetic field strength is set lower to $\omega_0/\omega = 0.49$, the resonance layer moves toward the helical coil so that the EC power can be deposited on-axis. The calculated power density is 9W/cm^3 for on-axis heating and 5W/cm^3 for off-axis heating.

3. Effect of Magnetic Field Ripple

There are two components in measured non-inductive current in ECH plasmas; bootstrap current and EC driven current. The exclusion of bootstrap current is required for accurate estimation of the EC driven current. One method is to use their different dependence on the magnetic field direction. The bootstrap current, which is proportional to $\mathbf{B}\times\nabla B$ drift, changes the flowing direction when reversing the magnetic field, while that of the EC current associated with the B strength does not change its flowing direction. Magnetic field reversal experiments have been conducted in Heliotron J in order to separate the EC current from the bootstrap current. We confirmed that the global plasma parameters such as stored energy and T_e did not change when reversing the magnetic field direction. Neither strong confinement degradation nor MHD instabilities were

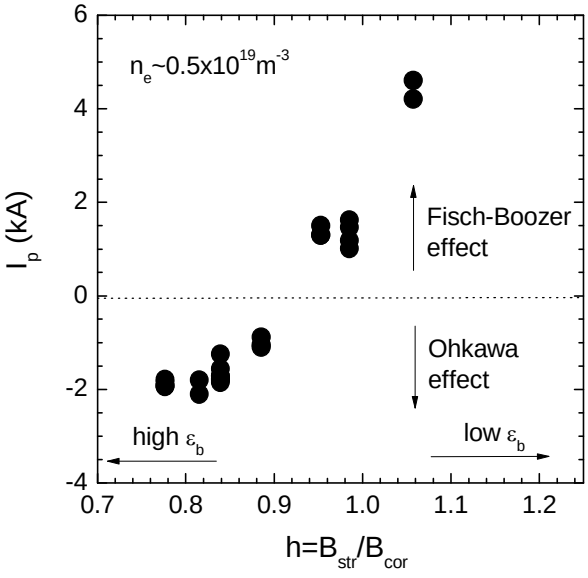

FIG. 2. Dependence of measured toroidal current on magnetic field ripple. The EC driven current is a main contribution to the toroidal current.

observed in the experiment reported here. The amplitude of bootstrap current agrees with a neoclassical prediction [16]. The bootstrap current is less than 0.5 kA at low density, which is smaller than the EC driven current, so that the toroidal current is mainly driven by ECCD.

Figure 2 shows the measured toroidal current as a function of the magnetic field ripple at n_e=0.5×10^{19} m^{-3}. Here the positive sign of the current corresponds to the direction determined by the Fisch-Boozer effect. The Ohkawa effect, on the other hand, drives the current in the negative direction. The EC driven current flows in the Fisch-Boozer direction when the EC power is deposited at the ripple top position. As the EC power is deposited at the deeper ripple bottom position, the EC driven current goes to zero, and then changes its flowing direction.

One reason for current reversal is that velocity space effects are responsible for ECCD. The Fisch-Boozer effect considers the perpendicular excursion in the velocity of a group of electrons with positive $v_{\|}$ [17]. Acceleration of these electrons causes an excess of electrons with counter-clockwise $v_{\|}$, resulting in a current in the clockwise toroidal direction. On the other hand, the Ohkawa effect drives current in the opposite direction to the Fisch-Boozer current [18]. Asymmetry in $v_{\|}$ is lost due to the bounce in the magnetic ripple, and a deficit in velocity space generates an electrical current in the counter-clockwise toroidal direction. In the ripple bottom heating, the electrons are accelerated in the valley of the ripple, and they tend to become trapped, thus enhancing the Ohkawa effect. These qualitative predictions are consistent with the experimentally measured ECCD direction. The Ohkawa effect has comparable strength to the Fisch-Boozer effect in S/H systems, and the ECCD direction is determined by the balance between them.

Measurement results on X-ray spectrum with a PHA system support this hypothesis. The SX spectra measurement indicates that the electrons with the energy more than 4 keV are enhanced when the EC power is deposited on magnetic axis at the ripple top position, while

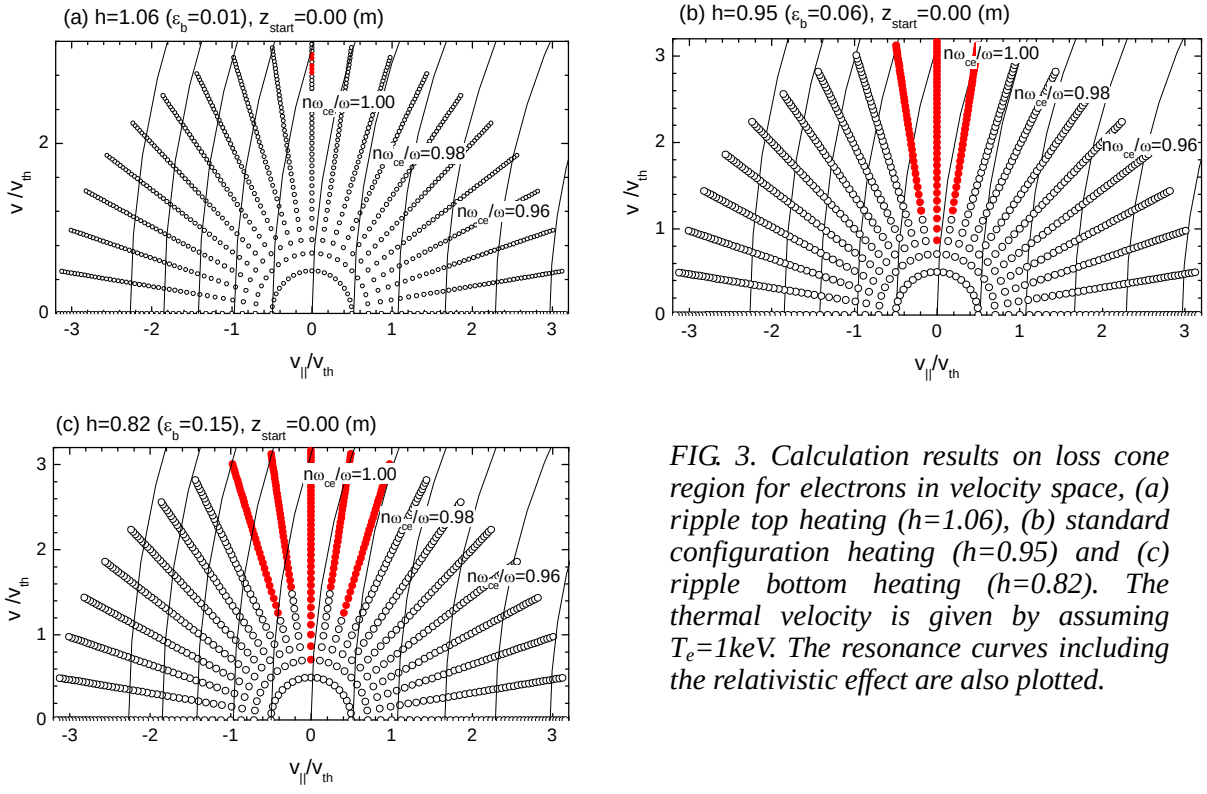

FIG. 3. Calculation results on loss cone region for electrons in velocity space, (a) ripple top heating (h=1.06), (b) standard configuration heating (h=0.95) and (c) ripple bottom heating (h=0.82). The thermal velocity is given by assuming T_e=1keV. The resonance curves including the relativistic effect are also plotted.

no such a high energy is observed at the ripple bottom heating. The VUV spectrum measurement using a polychrometer confirmed that the main impurity intensities were almost unchanged for both magnetic field strengths.

Non-appearance of high energy tail at the ripple bottom heating is possibly related to the confinement of trapped electrons. Loss cone region for electrons in velocity space is calculated by tracing electron trajectories. We assume that the electrons start from the magnetic axis at the straight section where the EC power is injected. Figure 3 shows the calculation results on the loss cone region. Three magnetic field configurations are considered; ripple top heating (h=1.06), standard configuration heating (h=0.95) and ripple bottom heating (h=0.82). We defined that the electron is lost when it reaches the last closed flux surface. The calculation is stopped at the time period, Δt=400 μsec, which is comparable to the electron-ion collision time, τ_{ei}=200 μsec for n_e=0.4×10^{19} m^{-3}, T_e=1 keV and Z_{eff}=1. It can be seen that the loss cone region expands with decreasing the ripple parameter, h. This means that for ripple bottom heating, the electron with large $v_\perp$ are trapped in the magnetic ripple, and then they are lost from the confinement region. These calculation results explain that the Ohkawa effect is stronger in the ripple bottom heating. The trapped region in velocity space will be investigated in the near future. The dependence of single particle confinement on the magnetic field configuration has a contrast with the global energy confinement experimentally observed in high-density regime, that is, the stored energy is higher in the ripple top heating and standard configuration heating. This is because the global confinement could be determined by the whole magnetic field structure.

4. Dependence on Resonance Position

Motojima, et al. reported that the ECCD was enhanced when the EC power was deposited on axis [5]. We have extended the configuration types, and have studied the dependence on the resonance position. Figure 4 shows the observed toroidal current as a function of ω_0/ω. The electron density was set as low as n_e = 0.5×10^{19} m^{-3} so that the EC current would be dominant. Since the B contour has a saddle-type structure, the resonance layer moves vertical at ω_0/ω > 0.49, in the poloidal cross-section. I_p is nearly zero at the off-axis low field side heating (ω_0/ω>0.50), and it increases as the resonance position reaches the magnetic axis. In the ripple bottom heating of h=0.82 and 0.89, the current has maximum negative current at ω_0/ω = 0.49, and the standard configuration heating has a similar result as h=0.95 case. Note that I_p data is not available at ω_0/ω<0.49 for ripple top heating because no plasma breakdown occurs by second harmonic ECH due to low single-pass X-mode fraction. Plasma is easily produced at ripple top heating because the fundamental resonance appears inside the vacuum chamber.

The dependence of ECE intensity on the magnetic field strength is examined as shown in Fig. 5. The ECE signal is measured with a 16-channel heterodyne radiometer. The central ECE channel is chosen for each configuration, and the intensity is normalized by that at ω_0/ω=0.5. Note that the resonance shift is small, $\Delta\rho$<0.05, for 0.48<ω_0/ω<0.50 at the ECE diagnostic port where the mod B has steep gradient. The optical thickness for the ECE diagnostic is grey, τ~1, for n_e=0.5×10^{19} m^{-3}, T_e=500 eV, so that the ECE signal reflects the contribution from both thermal and high-energy electrons. The ECE intensity is significantly increases at on-axis heating for ripple top heating, and the ECE intensity is sensitive to the electron density particularly at low-density regime. On the other hand, the increase is modest for ripple bottom heating, and it is kept nearly constant independent of electron density.

The magnetic axis shift has been performed by changing the outer vertical coil current in order to investigate the relationship between the resonance position and the magnetic axis. Figure 6 shows I_p as a function of the magnetic axis position. The magnetic configuration with ripple top heating (h=1.06) is selected. The maximum I_p is achieved when the magnetic axis is located at R_{axis}=1.076 m. According to HINT2 code calculation results, the magnetic axis shift due to finite beta (β_0=0.5 %) is ΔR=5 mm, while the shift due to the ECCD (I_p=±5 kA) is small, ΔR=1 mm. No change in peak position is observed when the EC injection angle is slightly tilted ~1 deg in the poloidal direction, that is, the beam position shifted from R_{axis} =1.070 m to R_{axis}=1.081 m. The beam size is relatively large, 60 mm in $1/e^2$ power at the equatorial plane. These suggest that the current drive region is mainly determined by the beam shape, and its peak is determined by the resonance layer position. The magnetic field for maximum I_p is 1.216 T, corresponding that the resonant electrons have the energy of around 2 keV under the resonance condition including the relativistic effect.

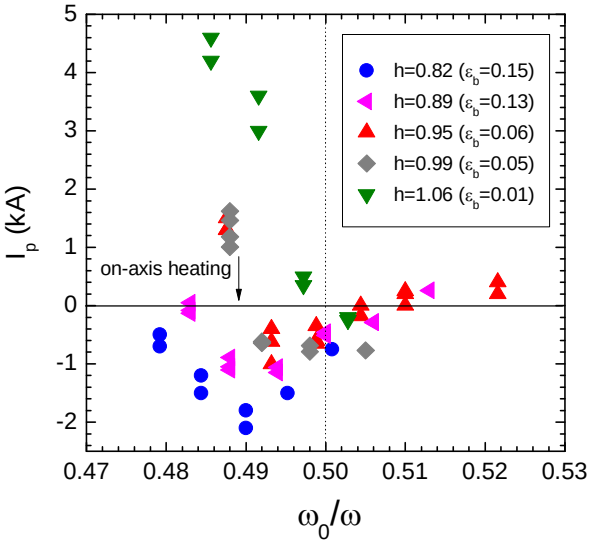

FIG 4. Dependence of I_p on magnetic field strength. The electron density is 0.5×10^{19} m^{-3}.

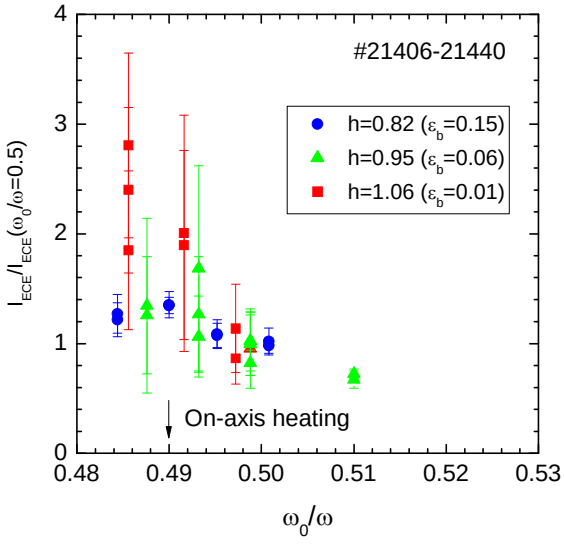

FIG 5. Dependence of ECE intensity on magnetic field strength. The intensity is normalized by that at ω_0/ω=0.5 for each configuration. The electron density range is $0.3\text{-}0.6\times10^{19}$ m^{-3}.

5. ECCD Efficiency

The ratio of driven current to injection power, I_{EC}/P_{EC}, and the figure of merit, $\gamma=n_e I_{EC}R/P_{EC}$, are conventionally used for the estimation of ECCD efficiency. The drawback of these functions is that they have dimension, and they do not reflect the T_e dependence. A figure of merit describing dimensionless ECCD efficiency including the T_e dependence is proposed in the form of $\zeta = e^3 n_e I_{EC}R/\varepsilon_0^2 P_{EC}T_e = 32.7 n_e I_{EC}R/P_{EC}T_e$ [3] where parameters have a unit of n_e in 10^{20} m^{-3}, I_{EC} in A, R in m, P_{EC} in W, and T_e in keV. This dimensionless figure of merit includes important parameters such as n_e and T_e. If ζ changes under the same plasma conditions, it means that ζ reflects the effect of electron thermal velocity and trapping.

Figure 7 shows the dependence of I_p on $P_{abs}T_e/32.7Rn_e$ at $n_e=0.4\text{-}0.6\times10^{19}$ m^{-3}. Here the absorbed EC power is estimated by the injected EC power and single pass absorption estimated by a transmitted wave measurement. The slope gives the normalized ECCD efficiency, ζ. With an increase of absorbed EC power from 110 kW to 440 kW, the EC driven

current increases from -0.3 kA to -2.5 kA for the ripple bottom heating, and it increases from 0.8 kA to 3.0 kA for the ripple top heating. The normalized ECCD efficiency is 0.020 and -0.018 for the ripple top and bottom heating cases, respectively. ζ is not maximal for the ripple top heating since the magnetic field is set a little higher, $\omega_0/\omega = 0.495$ for a wide power scan. Although ζ is independent of the EC power for both ripple top and bottom heating cases, the behavior of γ is a little different. In the ripple top heating, γ increases from 0.35×10^{17} A/Wm^2 to 0.5×10^{17} A/Wm^2 with increasing EC power, and T_e also increases from 0.5 keV to 0.7 keV, resulting in almost constant ζ. Effective confinement of high energy electrons may increases bulk electron temperature in low-density regime. In the ripple bottom heating, on the other hand, γ slightly increases from γ=-0.25×10^{17} A/Wm^2 to -0.3×10^{17} A/Wm^2, and the increase in T_e is weak, 0.45 keV to 0.55 keV. This power scan result suggests that ζ is constant when the magnetic field ripple structure is fixed. Although ζ should include the effect of impurities, Z_{eff} is not measured yet in Heliotron J. Study on the effect of impurities on ζ is left for future.

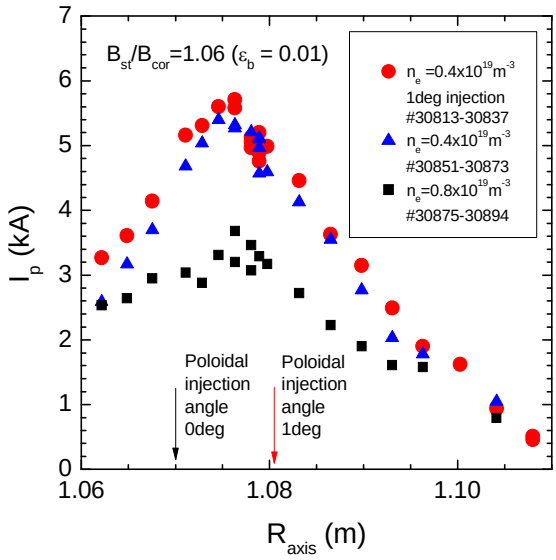

FIG. 6. Dependence of I_p on magnetic axis shift for ripple top heating.

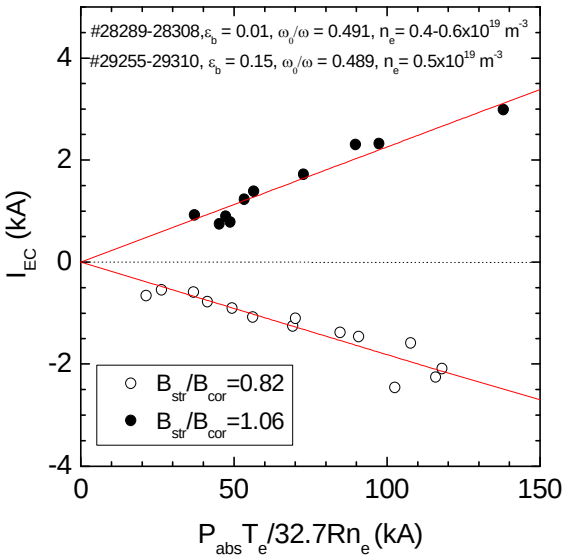

FIG. 7. Dependence of EC driven current on $P_{abs}T_e/32.7Rn_e$.

Recent international collaboration research on ECCD in Heliotron J, TJ-II and CHS has shown that the maximum EC current amount is a few kA in all the devices, and the ECCD efficiency is similar, ζ=0.03-0.05 [10]. Although the magnetic field structure is different among the devices, the EC current amount is a few kA in all the devices, and the ECCD efficiency is the same order within a factor of 2. Rather low efficiency compared to tokamaks may be due to the strong Ohkawa effect enhanced by the magnetic ripple. Although such an ECCD efficiency is about 10 times lower than that in tokamak device, it is comparable to the bootstrap current and NBCD current, suggesting that the ECCD is applicable for cancellation of other non-inductive current, thus tailoring the rotational transform profile.

6. Conclusion

The ECCD experiments have been conducted in Heliotron J, focusing on the effect of magnetic field ripple. The experiments scanning the magnetic field configuration show that

the EC driven current decreases as the power is deposited at deeper magnetic field ripple bottom. The reversal of driven current direction is observed as the power is deposited at ripple bottom, indicating that the amplitude and direction of EC current is determined by the balance between the Fisch-Boozer effect and the Ohkawa effect. The measurement results and the calculation of electron loss in velocity space indicate that the reduction in EC driven current is related to the generation and confinement of trapped electrons. The maximum current ever observed is 6 kA, and the ECCD efficiency is $\gamma=n_e I_{EC} R/P_{EC}=8\times10^{16}$ A/Wm^2, $\zeta=32.7 n_e I_{EC} R/P_{EC} T_e=0.05$. Low efficiency compared to tokamaks may be due to the strong Ohkawa effect enhanced by the toroidal and helical ripples.

While the ECCD efficiency is not so high, the EC current is comparable to the bootstrap current, meaning that we are able to control the total toroidal current. The EC current is comparable to the bootstrap current, and the ECCD has a potential to control the rotational transform profiles. Since the bootstrap current profile should be different from the EC current profile, we will need to extend the control ability from the viewpoint of the modification of rotational transform closely connected to the suppression of MHD instabilities. A ray tracing calculation code taking the 3D ripple structure into account is under development, which will clarify the role of trapped electrons by comparing between experiment and theory.

Acknowledgements

The authors are grateful to the Heliotron J staff for conducting the experiments. This work was supported by NIFS/NINS under the NIFS Collaborative Research Program (NIFS04KUHL005) and under a project sponsored by the Formation of International Network for Scientific Collaborations.

References

[1] G. Motojima, et al., Plasma and Fusion Res. **3** (2008) S1067.
[2] T. Mizuuchi, et al., Nucl. Fusion **47** (2007) 395.
[3] S. Kobayashi, et al., 11th IAEA TM on H-mode Phys. Trans. Barriers (Tsukuba, 2007).
[4] K. Nagasaki, et al., Nucl. Fusion **45** (2005) 1608.
[5] G. Motojima, et al., Nucl. Fusion **47** (2007) 1045.
[6] V. Erckmann, et al., Nucl. Fusion **43** (2003) 1313.
[7] A. Fernandez, et al., Fusion Sci. and Tech. **53** (2008) 254-260.
[8] Y. Yoshimura, et al., Fusion Sci. Technol. **53** (2008) 54-61.
[9] T. Notake, et al., Plasma and Fusion Res. **3** (2008) S1077.
[10] K. Nagasaki, et al., Plasma and Fusion Res. **3** (2008) S1008.
[11] M. Wakatani, et al., Nucl. Fusion **40** (2000) 569-573.
[12] T. Obiki, et al., Nucl. Fusion **41** (2001) 833.
[13] K. Nagasaki, et al., Plasma Fusion Res. **2** (2007) 039.
[14] V. Tribaldos *et al.*, Plasma Phys. Control Fusion **40** (1998) 2113.
[15] Á. Cappa, et al., Plasma and Fusion Res. 2 (2007) 030.
[16] G. Motojima, et al., Fusion Sci. Technol. **51** (2007) 122.
[17] N. J. Fisch and A. Boozer, Phys. Rev. Lett. **45** (1980) 720.
[18] T. Ohkawa, General Atomics Report GA-A13847 (1976).